Pressure-Based Assessment of SST-IDDES for Surface Pressure and FIV-Relevant Metrics in Staggered Tube-Bundle Cross-Flow

Bumjin Cho, Minseop Song*
Department of Nuclear Engineering, Hanyang University, 222, Wangsimni-ro, Seongdong-gu, Seoul, 04761, Republic of Korea
**Corresponding author: hysms@hanyang.ac.kr*

Keywords : Staggered tube-bundle, LES, DES, Surface pressure coefficient, Fluid-induced vibration

1. Introduction

Small modular reactors (SMR) are being developed as next-generation nuclear systems, offering enhanced safety and flexible operating characteristics compared with large-scale nuclear power plants. The compact design of SMR requires high heat-transfer performance within a limited space, and helical coil steam generators (HCSG) are widely considered a high-efficiency configuration to meet this demand. However, the tube-bundle arrangement in an HCSG, characterized by tube rows oriented and intersecting perpendicular to the main flow direction, induces complex cross-flow through the bundle. This cross-flow can lead to strong flow separation, wake interactions, and amplified turbulent structures, thereby increasing flow unsteadiness and the risk of flow-induced vibration (FIV). Therefore, it is crucial to establish robust analysis and validation frameworks that can quantitatively evaluate the unsteady loads acting on tube surfaces during the design stage and secure sufficient safety margins for long-term operational reliability.

The cross-flow problem in tube-bundles has traditionally been analyzed using RANS-based models, such as the SST k–ω, which predict the mean flow field and pressure drop at a relatively low computational cost [1]. However, key FIV related quantities, including unsteady vortex shedding, low-frequency large-scale structures, and wall-pressure fluctuations, are often excessively damped due to the time-averaged closure nature of RANS. Accordingly, LES is recognized as a high-fidelity approach that can reproduce turbulent structures and unsteady statistics in a more physically consistent manner [2]. Nevertheless, for high Reynolds number flows and complex bundle geometries, LES requires very fine spatial and temporal resolution, leading to a sharp increase in computational cost, which limits its direct applicability to iterative design evaluations or broad parametric studies.

In this context, hybrid turbulence models such as detached eddy simulation (DES) have attracted attention as a compromise between cost and accuracy by treating the near-wall boundary layer with RANS while resolving separated wake regions at an LES-like level [3]. Previous studies have discussed DES-family approaches mainly using flow field-oriented metrics, such as wake structures and turbulence statistics [4]. However, quantitative validation of whether DES can achieve LES level fidelity for pressure- and load-based FIV metrics, which are directly linked to design loads, remains relatively limited. Because the impacts of near-wall RANS treatment and the RANS–LES transition characteristics inherent to Improved delayed detached eddy simulation (IDDES) on surface-pressure prediction have not been fully clarified, it is difficult to conclude that similarity in flow characteristics straightforwardly implies equivalence in pressure-based design metrics.

This study uses a wind-tunnel experimental dataset of tube-bundle surface pressure coefficients released by Trinity College Dublin as a benchmark [5]. Transient simulations are conducted for cross-flow over a 7×5 staggered tube-bundle using URANS (SST k–ω), LES (WALE), and DES (SST-IDDES). Model fidelity is evaluated by directly comparing the time-averaged circumferential pressure distribution of the central tube with experimental measurements. Since the benchmark provides only the time-averaged $C_p(\theta)$, the validation in this study is restricted to the mean circumferential pressure distribution of the central tube. Unsteady FIV-related metrics, including wall-pressure fluctuations, drag and lift statistics, and PSD-based peak frequencies, are then used to benchmark DES against LES. Through this pressure-based FIV-metrics framework, this work aims to identify the applicability and limitations of DES and provide an evidence-based workflow to support turbulence-model selection for SMR HCSG design.

2. Experimental Benchmark

This study uses a wind-tunnel benchmark dataset reported and released by Mahon and Meskell (2009). As shown in Fig. 1, the experiments were conducted in a 750 mm-long draw-down wind tunnel test section with a 300 mm × 300 mm cross-section, where a five-row staggered tube array was installed and tube surface pressure coefficients were measured under air cross-flow conditions [5]. The free-stream velocity was measured upstream of the array using a pitot-static tube and a micromanometer; the inlet velocity range was 2–18 m/s and the free-stream turbulence intensity was below 1%. The tube diameter was 38 mm, and the instrumented central tube had 36 pressure taps (1 mm diameter) located at the mid-span and distributed circumferentially

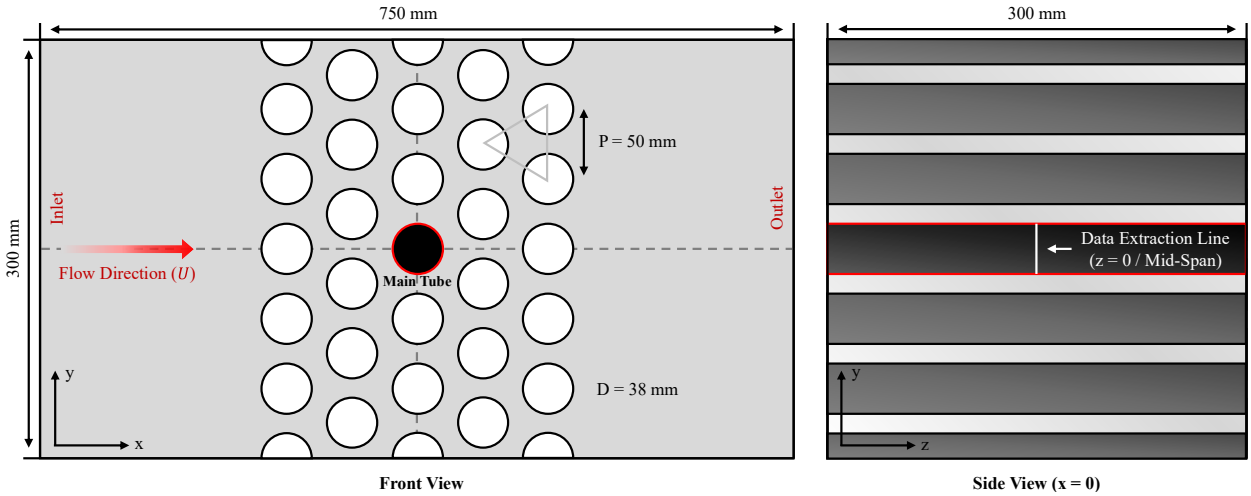

Fig. 1. Test-Section Schematic; P/D=1.32

at 10° intervals to acquire surface pressure (see Fig. 2). Pressure signals were sampled at 64 Hz and time averaged to obtain the mean pressure and pressure-coefficient distributions; the released dataset provides the circumferential C_p distribution. The C_p was defined using the gap velocity U_g as

$$C_p(\theta) = 1 - \frac{P_{\theta,max} - P_\theta}{\frac{1}{2}\rho U_g^2}, \quad (1)$$

where P_θ is the time-averaged static pressure at the circumferential position θ and $P_{\theta,max}$ is the maximum value over θ.

The condition $P/D = 1.32$ and $U = 7\ m/s$ ($U_g = 29.2\ m/s, Re = 7.82 \times 10^4$) was selected as the representative case from Reference [5]. For validation, the time-averaged circumferential C_p distribution $C_p(\theta)$ at $z = 0$ (mid-span) on the central tube was adopted as the primary metric, and CFD results were directly compared with the experimental data following the angle definition in Fig. 2. In addition, LES and DES were compared using FIV-relevant metrics, including surface-pressure fluctuations and the statistical and spectral characteristics of drag and lift loads, to assess the applicability and limitations of DES from the FIV metrics perspective.

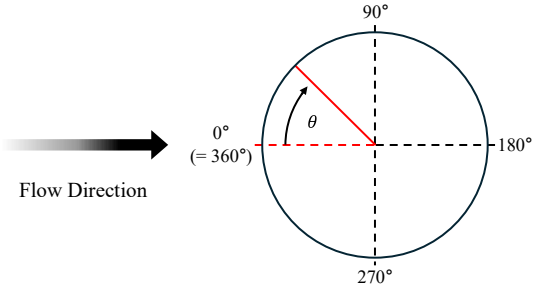

Fig. 2. Schematic of position angle

As illustrated in Fig. 3, the front-side stagnation region is located near θ = 0°, separation typically occurs around θ ≈ 90° and 270°, and the wake/recirculation region associated with pressure recovery lies near θ ≈ 180°.

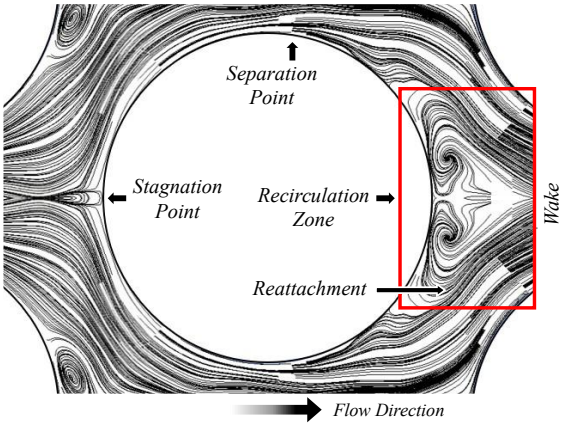

Fig. 3. Schematic of key mean-flow features around the central tube in staggered tube bundle cross-flow

3. Numerical Details

In this section, the numerical methods used to reproduce the tube-bundle cross-flow benchmark are described. The numerical details include the computational domain and boundary conditions, solver setup, and turbulence models for URANS, LES, and DES. The grid system and resolution criteria are also presented, including y^+, the LES m-value, and a URANS grid-sensitivity study to support solution reliability.

3.1 Computational Domains and Boundary Conditions

Based on previous research, the spanwise (z) domain width was reduced to one-third of the experimental test-section width because its influence on the mid-span pressure field was considered limited [6]. To avoid artificial side-wall effects in the reduced-width domain,

the lateral boundaries were set to periodic, while all remaining walls (including tube surfaces) were treated as no-slip. The wake length was extended for LES and DES to better capture wake-driven unsteady effects, and the inlet turbulence intensity was set to 1% to match the benchmark condition.

3.2 Computational Setup

All simulations were performed using a pressure-based, incompressible formulation because compressibility effects are negligible for the present low-speed, isothermal air flow. URANS employed the Coupled algorithm, while LES and DES used PISO for transient integration. Time stepping and statistical sampling settings are summarized in Table I. The statistics window of 0.2s was selected as the minimum duration that includes approximately 50 cycles of the dominant unsteady motion, based on the URANS (Coarse) reference.

Table I: Summary of Computational Setup

	URANS	LES	DES
Model	SST *k–ω*	WALE	SST-IDDES
Solver Formulation	Pressure-based, Incompressible		
P-V Coupling	Coupled	PISO	PISO
Momentum Discretization	2nd-order upwind	Bounded central differencing	Bounded central differencing
Time step	1e-04 s	2e-05 s	2e-05 s
Burn-in (Discarded)	0-0.04s	0-0.04s	0-0.04s
Statistics window	0.04-0.24s (Total 0.2s)	0.04-0.24s (Total 0.2s)	0.04-0.24s (Total 0.2s)

3.3 Turbulence Models

To examine model sensitivity, this work considers URANS (SST *k–ω*), LES (WALE), and DES (SST-IDDES). SST *k–ω* is used as a low-cost baseline for predicting the mean flow and mean pressure fields, while LES with WALE is adopted as the high-fidelity reference to resolve near-wall turbulence and unsteady wake dynamics affecting surface-pressure fluctuations. SST-IDDES is SST *k–ω* based hybrid RANS–LES method that applies RANS in the near-wall region and LES-like resolution in separated and wake regions, with shielding and transition treatments aimed at reducing grid sensitivity and undesired boundary layer mode switching. Prior studies have reported acceptable agreement between DES and LES, motivating its use here to assess cost–accuracy trade-offs for FIV metrics.

3.4 Grid System and Resolution Criteria

All meshes were generated using hexa-dominant cells, and separate grid systems were prepared for URANS, LES, and DES to meet model-specific resolution requirements. Table II summarizes the total cell count and near-wall metrics, including y^+ and the growth ratio.

Table II: Mesh Information for Each Models

		# of Cells	y^+	Growth Rate
URANS	Fine	9,064,650	< 0.8	1.18
	Medium	6,402,912	< 0.8	1.21
	Coarse	3,954,780	< 0.8	1.29
LES		9,962,400	< 0.6	1.18
DES		7,480,520	< 0.9	1.20

For LES, the grid was designed to keep the fraction of subgrid-scale turbulent kinetic energy relative to the total below the recommended limit. The m-value is defined as follows:

$$m = \frac{k_{sgs}}{k_{sgs} + k_{resolved}} < 0.2 \qquad (2)$$

In this study, the LES mesh was conservatively refined to satisfy $m < 0.05$.

Because cross-flow over a tube-bundle is inherently unsteady, a grid-sensitivity study was conducted using time-averaged statistics from unsteady RANS simulations rather than steady-state results. Table III reports the sensitivity of the pressure drop for the URANS Fine/Medium/Coarse meshes. Because pointwise percentage differences can be exaggerated where C_p approaches zero, grid convergence for the mean $C_p(\theta)$ was assessed primarily by the similarity of the overall profile and the locations of the main extrema (Fig. 4). However, the PSD-based frequency analysis in Fig. 5, obtained from the angle averaged surface pressure spectra, shows that the coarse grid shifts the dominant peak to a much lower frequency (≈ 242 Hz), whereas the fine and medium grids exhibit comparable dominant peaks in a similar band (≈ 430–445 Hz).

Table III: Calculated ΔP and Relative Discrepancy

	Pressure Drop [Pa]	Discrepancy [%]
Fine	822.851	-
Medium	823.942	+ 0.13
Coarse	874.669	+ 6.30

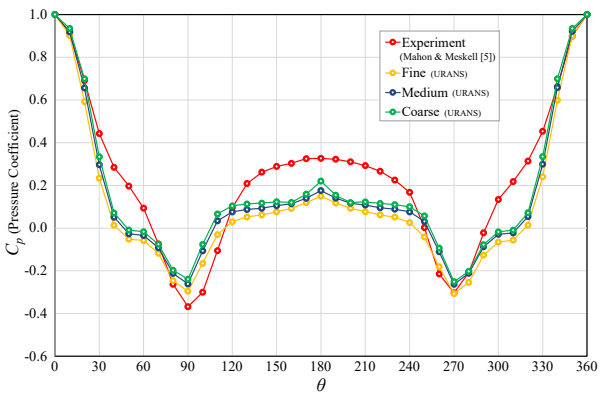

Fig. 4. $C_p(\theta)$ on the central tube: experiment vs URANS grid resolution

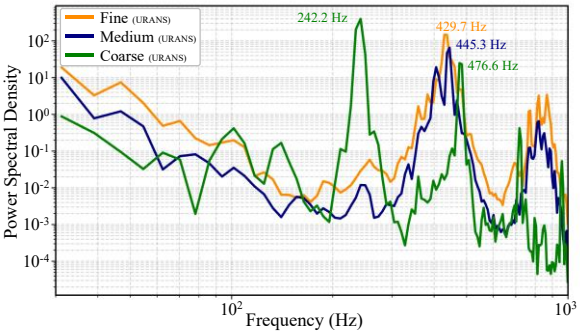

Fig. 5. Angle-averaged surface-pressure PSDs for URANS grid refinement study

Finally, the DES mesh was designed to promote smooth IDDES mode switching in the separated region by combining URANS-Medium near-wall quality with LES-like resolution in the key wake region. Fig. 6 shows the final DES mesh used in this study.

4. Results and Discussion

4.1 Validation of Mean Surface Pressure Coefficient

The mean circumferential surface pressure coefficient $\bar{C_p}(\theta)$ on the central tube was compared with the wind-tunnel data and the predictions of URANS (Fine), LES, and DES using the same angular definition shown in Fig. 7. Overall agreement is consistent near the stagnation region ($\theta \approx 0°$), while larger discrepancies appear in separation and wake sensitive regions. LES captures the pressure-recovery trend more consistently around $\theta \approx 180°$, whereas DES underpredicts the recovery and shows a profile similar to URANS. This trend is supported by the error quantification in Table IV, where LES yields the smallest discrepancy to the experiment (RMSE=0.070, MAE=0.055), while DES and URANS show larger errors (RMSE=0.179, 0.165) with negative mean bias, indicating systematic underprediction in the wake-side pressure recovery.

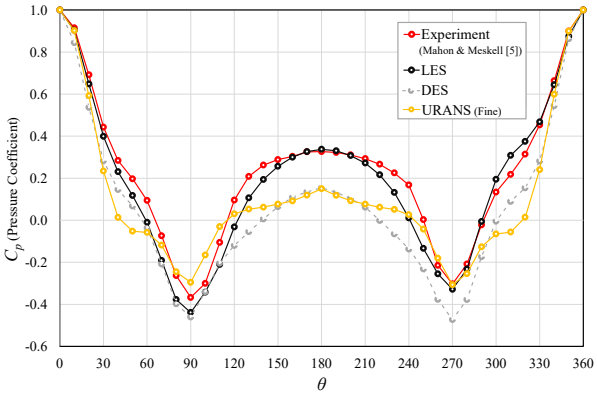

Fig. 7. $C_p(\theta)$ on the central tube: Experiment vs LES, DES, and URANS(Fine)

Table IV: Quantitative Error of $\bar{C_p}(\theta)$ Relative to Experiment

Model	LES	DES	URANS
RMSE	0.070	0.1786	0.1645
MAE	0.0550	0.1648	0.1392
Mean Error	-0.0404	-0.1648	-0.1205
Max |Δ|	0.1573	0.3048	0.3000
Angle at Max |Δ|	240°	240°	320°

4.2 Comparison of Mean Velocity Profile

To examine a possible cause of the wake-related discrepancy in $\bar{C_p}$, thirteen monitoring points were placed along the flow passage around the central tube as illustrated in Fig. 8. The time-averaged velocity magnitude $\overline{V_{mag}}$ at these locations indicates noticeable model-dependent differences between LES and DES (Fig. 9), suggesting differences in wake recovery/mixing and gap-jet diffusion. These differences in the mean flow field provide a plausible link to the underpredicted pressure recovery near $\theta \approx 180°$ observed in the mean C_p comparison.

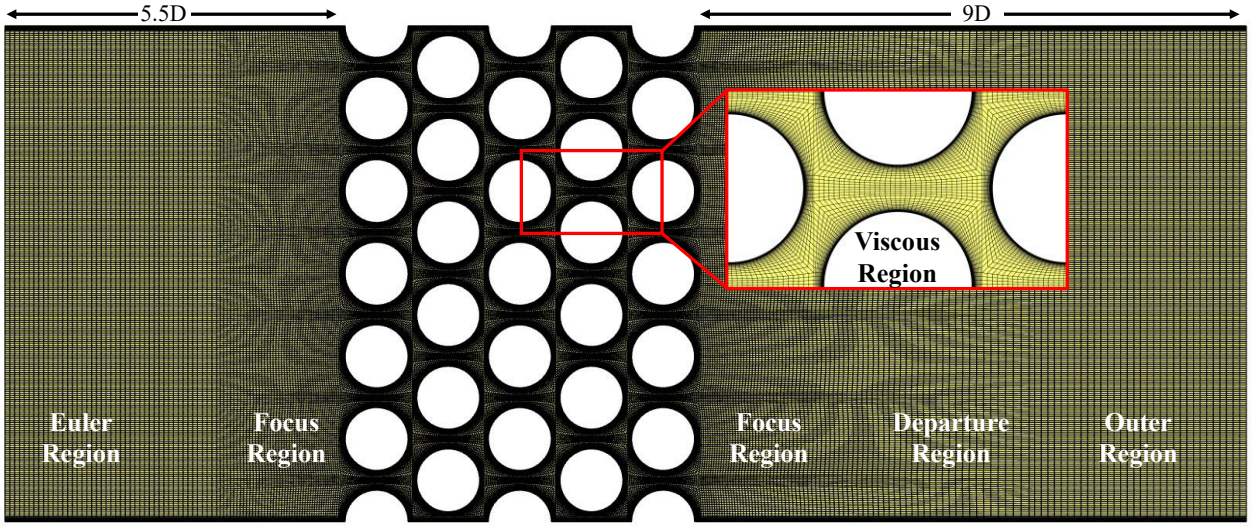

Fig. 6. DES Grid Topology for the Staggered Tube-Bundle, with a Close-up of the Viscous region

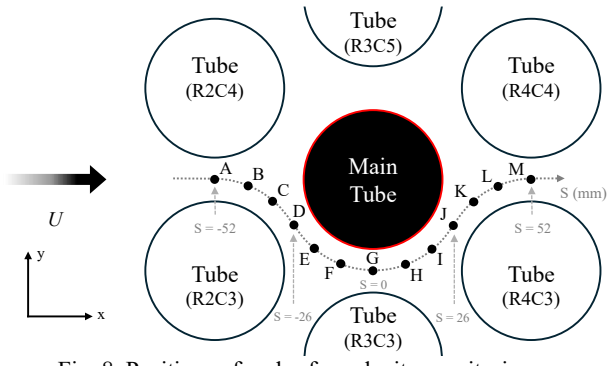

Fig. 8. Positions of nodes for velocity monitoring; S = Curvilinear Coordinate

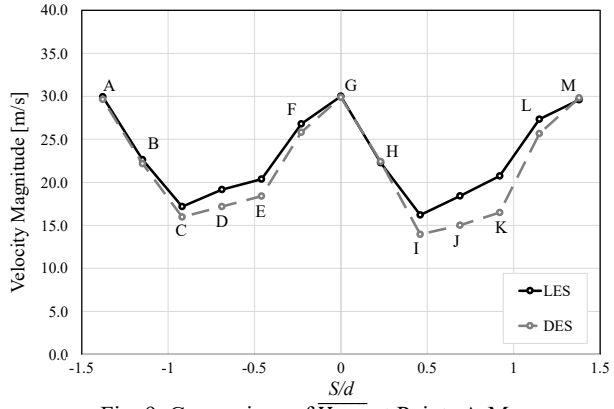

Fig. 9. Comparison of $\overline{V_{mag}}$ at Points A-M

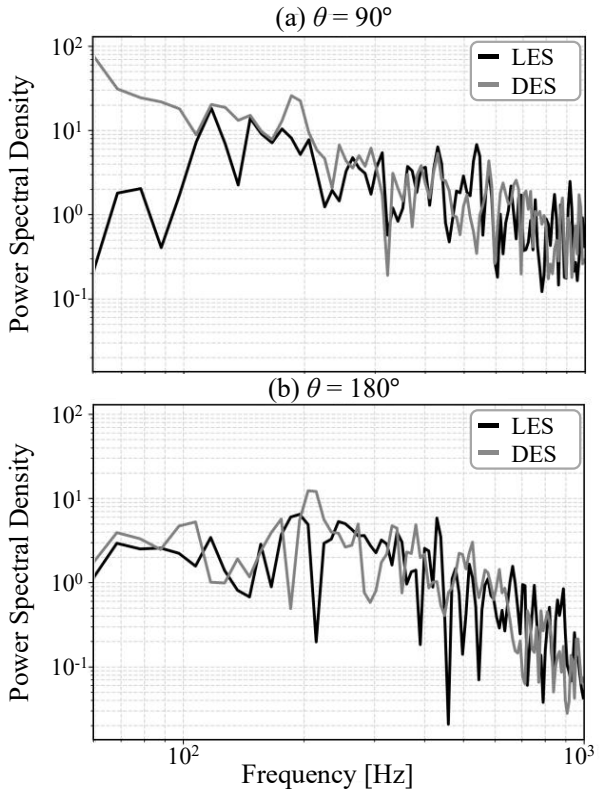

Fig. 10. Wall-Pressure PSD Comparison at $\theta = 90°$ (a) and $180°$ (b)

4.3 Spectral Characteristics

The unsteady wall-pressure characteristics were assessed through PSD analysis using the static-pressure time series extracted at representative circumferential locations on the central tube. The PSD results at $\theta = 90°$ and $\theta = 180°$ are presented in Fig. 10 to compare the separation- and wake-sensitive regions between LES and DES. For a non-dimensional comparison, the dominant peak frequency f_{peak} was converted to the Strouhal number using $St = f_{peak}\, D/U_g$, where D = 38 mm and $U_g = 29.2$ m/s. The dominant peak was identified within the 50–1000 Hz band.

Although DES shows a larger discrepancy in the mean C_p near $\theta \approx 180°$ in Fig. 7, the dominant peak frequencies remain similar. The dominant peaks are 195.31 Hz (St = 0.254) for LES and 205.08 Hz (St = 0.267) for DES. Differences at $\theta = 90°$ further indicate model-dependent unsteady behavior even when the mean C_p is similar. Consistent with Fig. 7 where LES and DES show similar mean C_p near $\theta \approx 90°$, the PSD-based dominant peak still differs, with LES $f_{peak} = 117.19$ Hz (St = 0.153) and DES $f_{peak} = 58.59$ Hz (St = 0.076), suggesting a stronger low-frequency contribution in DES in the separation-sensitive region.

4.4 Statistical Comparison of Force Coefficients

The integrated aerodynamic loads on the central tube were compared using the drag and lift coefficients to provide additional FIV-relevant metrics. Because the force records contain a limited number of samples (N = 201) over T = 0.2 s with $\Delta t = 0.001$ s, the comparison is based on mean and fluctuation statistics (RMS and peak-to-peak) rather than PSD, as summarized in Table V. Peak-to-peak values are sensitive to record length and intermittent extreme events, and are therefore reported as a complementary indicator alongside RMS. The mean drag $\bar{C}_d$ is nearly identical between LES and DES, while DES shows larger drag fluctuations; lift fluctuation RMS levels are similar, but DES exhibits a larger peak-to-peak lift excursion. The mean lift is reported as $|\,\bar{C}_l\,|$ to emphasize load magnitude rather than direction.

Table V: Central Tube Force-Coefficient Statistics

Metric	LES	DES	Discrepancy
Mean Drag Coefficient	1.139	1.141	0.2 %
RMS Drag Fluctuation	0.109	0.120	10.1 %
Peak-to-peak drag fluctuation	0.622	0.843	35.3 %
Mean Lift Coefficient	0.072	0.051	29.2 %
RMS Lift Fluctuation	0.216	0.222	2.8 %
Peak-to-peak lift fluctuation	0.943	1.241	31.6 %

4.5 Additional Verification

Since the present results are based on a high Reynolds number operating condition ($U = 7$ m/s, $Re = 7.82 \times 10^4$), additional verification is required to generalize the applicability of DES. In particular, (i) a longer statistical window should be secured to assess low-frequency fluctuations and the convergence of mean quantities, (ii) the same metrics should be re-evaluated under a lower-velocity/lower-Re condition (e.g., U = 2-3 m/s), and (iii) sensitivity studies should be conducted for DES with respect to wake-region resolution and the RANS–LES transition behavior. In addition, validation against available reference datasets is planned for lower-inlet-velocity conditions and additional P/D configurations. particle image velocimetry (PIV) based validation is also planned for representative cases to assess wake and gap-flow predictions. These efforts will help separate the underlying causes of the underpredicted pressure recovery near $\theta \approx 180^\circ$ and clarify the applicability range of DES.

5. Conclusions

This study examined whether DES can serve as a cost-effective alternative to LES for pressure- and FIV-relevant assessment of staggered tube-bundle cross-flow, using a wind-tunnel benchmark. Unlike many DES validations that primarily rely on velocity-field comparisons, the present work emphasizes surface-pressure-based validation and FIV-based unsteady metrics that are directly linked to design loads. Because the benchmark provides only time-averaged data, the mean circumferential surface pressure coefficient of the central tube was adopted as the primary validation metric, and LES, DES, and URANS were compared under identical conditions.

The mean pressure-coefficient distribution shows close agreement near the stagnation region, while clear model dependence appears in separation- and wake-sensitive regions. LES reproduces the pressure-recovery trend around $\theta \approx 180^\circ$ more consistently, whereas DES underpredicts the recovery and yields a profile closer to URANS. Mean velocity comparisons indicate noticeable LES-DES differences in wake recovery/mixing and gap-jet diffusion, which plausibly contribute to the reduced pressure recovery in DES. Wall-pressure PSDs at $\theta = 90^\circ$ and $\theta = 180^\circ$ further reveal different spectral energy distributions, and force statistics indicate nearly identical mean drag but larger fluctuation amplitudes in DES, with comparable lift RMS yet larger peak-to-peak lift excursions. Given that these observations are drawn from a single high-Re condition with a limited sampling window (0.04-0.24 s), DES should be applied conservatively for pressure-based FIV metrics in similar configurations, and additional validation and verification (V&V) are warranted before adopting DES-based predictions for design-relevant assessments in nuclear engineering, where conservative practice is required. Specifically, future V&V will include extended-time averaging for statistical convergence, validation under lower-inlet-velocity/lower-Re conditions and additional P/D configurations through comparison with reference datasets, PIV-based validation of the predicted flow field, and DES sensitivity studies on wake-region resolution and RANS–LES transition behavior.

Acknowledgements

This research was supported by the National Research Council of Science & Technology (NST) grant by the Korea government (MSIT) (No. GTL24031-000) and Innovative Small Modular Reactor Development Agency grant funded by the Ministry of Science and ICT(No. RS-2024-00408520).

REFERENCES

[1] Benhamadouche, S., Afgan, I. & Manceau, R. Numerical Simulations of Flow and Heat Transfer in a Wall-Bounded Pin Matrix. Flow Turbulence Combust 104, pp.19–44, 2020.
[2] S.J. Lee, Y.A. Hassan, Numerical investigation of helical coil tube bundle in turbulent cross flow using large eddy simulation, Int. J. Heat Fluid Flow pp.82, 2020.
[3] Mikhail S. Gritskevich, Andrey V. Garbaruk, Jochen Schütze, Florian R. Menter, Development of DDES and IDDES Formulations for the k-ω Shear Stress Transport Model. Flow Turbulence Combust 88, pp.431–449, 2012.
[4] Liu, K., Qiu, H., Wang, M., Zhang, J., Guo, K., Tian, W. & Su, G. Helium turbulent fluctuation characteristics in the multilayer helical tube bundle using improved delayed detached eddy simulation. Phys. Fluids 37, 035131, 2025.
[5] J. Mahon & C. Meskell. Surface pressure distribution survey in normal triangular tube arrays. Journal of Fluids and Structures 25, pp.1348–1368, 2009.
[6] Beatriz de Pedro, Jorge Parrondo, Craig Meskell & Jesús Fernández Oro. CFD modelling of the cross-flow through normal triangular tube arrays with one tube undergoing forced vibrations or fluid elastic instability. Journal of Fluids and Structures 64, pp.67–86, 2016.